In situ polyaniline polymerization on electrospun cellulose acetate nanofibers derived from recycled waste filter butts of cigarettes for the enhanced removal of methyl orange and rhodamine

In situ polyaniline polymerization on electrospun cellulose acetate nanofibers derived from recycled waste filter butts of cigarettes for the enhanced removal of methyl orange and rhodamine

Asabuwa Ngwabebhoh Fahanwi [a,b,*], Muhammad Yasir[a,], Hau Trung Nguyen[a], Nabanita Saha[a,b], Tomas Saha[b], Vladimír Sedlařík[a], Petr Saha[a,b]**

[a]*Centre of Polymer Systems, University Institute, Tomas Bata University in Zlin, Trida Tomase Bati 5678, 76001 Zlin, Czech Republic*

[b]*Footwear Research Centre, University Institute, Tomas Bata University in Zlin, Nad Ovcirnou IV, 3685, Zlin, Czech Republic*

**Corresponding author at: Centre of Polymer Systems, University Institute, Tomas Bata University in Zlin, Trida Tomase Bati 5678, 76001 Zlin, Czech Republic.*

***Corresponding author. E-mail addresses: asabuwa.nf@gmail.com (A.N. Fahanwi), yasir@utb.cz (M. Yasir).*

ABSTRACT

In this study, waste cigarette butts (CBs) were processed to produce electrospun cellulose acetate (CA) nanofibrous membranes modified with polyaniline ($PANI$) via chemical oxidation polymerization. This cost-effective method of preparing CA copatě with $PANI$ was initially investigated by comparing CA, $CA-PANI$, and $CA-dPANI$ (as deprotonated PANI) for the rapid adsorption of cationic and anionic dyes. The results depicted $CA-PANI$ with the highest dye removal capacity. As the optimum material, $CA-PANI$ was applied to remove methyl orange (MO) and rhodamine chloride (RC) dye from an aqueous phase. Essential factors: contact time, solution pH, initial dye concentration, nanofiber dosage, and temperature of solution were evaluated with maximum equilibrium adsorption capacity and removal percentage achieved for MO as 24.87 mg/g and 99 %, for RC as 6.93 mg/g and 55 %, respectively. The adsorptive experimental data for both dyes best fitted the pseudo-second-order kinetic, intraparticle diffusion, and Freundlich models. Moreover, the thermodynamics result indicated the adsorption processes were exothermic and spontaneous in nature. Reusability studies also showed the stable performance of $CA-PANI$ material for up to 7 adsorption-desorption cycles. The high dye removal efficiency suggests that the adsorbent material in the water filtration of azo dyes.

Keywords: Cellulose acetate, electrospinning, adsorption, polyaniline, oxidative polymerization, wastewater treatment

1. Introduction

More than 5.5 trillion cigarettes are reportedly fabricated annually around the world, and over 4.5 trillion waste filters of cigarette butts (CBs) are discarded improperly, resulting in about 2 million tons

of trash generated (**Shen et al., 2020; Torkashvand and Farzadkia, 2019**). Due to the global consumption of cigarettes, this poses serious health effects on human lives and the environment. The improper disposal of CBs in public spots such as bus stations, trains, tram stops, shopping malls, playgrounds, and parks (**Rebischung et al., 2018**) causes CBs to be regarded as crucial waste (**Bilge et al., 2019**). Disposed CBs contaminate soil and water, thereby deteriorating the biological, and chemical structure of the environment, leading to infertile land (**Montalvão et al., 2019; Torkashvand and Farzadkia, 2019**). In addition, CBs are non-degradable and, when improperly disposed of, pose a serious problem and significant damage to the ecosystem due to the accumulation of tobacco traces. CBs also affect marine life via human consumption thereafter flushed into lakes, rivers, and ultimately into the oceans (**Hemamalini et al., 2019**) (**Torkashvand et al., 2020**). Therefore, novel techniques for the recycling of CBs is required to reduce its improper disposal and pollution to the environment (**Alhokbany et al., 2020**).

To address this issue, several approaches have been explored, such as the development of materials from CBs for the remediation of water pollutants such as dyes and other related environmentally persistent toxicants in wastewater. Several treatment methods have been studied in the past, including advanced oxidation, photocatalysis, adsorption, biological degradation, and catalytic reduction (**Carvalho et al., 2017; Castellanos et al., 2021; Gao et al., 2020; Křesinová et al., 2018; Muhammad et al., 2022; Naz et al., 2021; Rafiq et al., 2021; Saleh, 2021a; Wei et al., 2018**). Amongst all, adsorption has emerged as the most advantageous technique due to several factors, such as effectiveness in the elimination of micropollutants; the process is fast, cheap, and facile (Saleh, 2021b). Additionally, the generation of harmful by-products, which occurs using other conventional methods, is avoided.

The composition of the adsorbent material is a predominant factor, which is ultimately essential for optimal performance. Activated charcoal granules (**Kumar et al., 2009; Kumar and Mohan, 2011**), fullerene (**Jin et al., 2007; Pan et al., 2008**), carbon nanotubes (**Kiran Kumar and Venkata Mohan, 2012**), chitosan, activated carbon adsorbents made from industrial waste (**Krupadam et al., 2011; Zhang and Zhou, 2005**) (**Hristovski et al., 2009**) are just a few of the adsorbents that have been reported in the literature. Due to their extensive surface area, these materials have proven to be effective at adsorbing water pollutants when dispersed in solution. However, they require a second step, which involves the removal of particles from residual water permeates, which hinders the usage of these materials in terms of cost-effectiveness. Whereas fibers, especially at submicron size, have recently attracted greater attention. This is because they possess distinctive properties, which include porous structure, high surface area, controlled fiber diameter, high aspect ratio, and lightweight (**Lu et al., 2022; Ma et al., 2022**). These characteristics allow significant solution contact and increase treatment efficiency. Additionally, it has been demonstrated that polymeric materials as fibers make appropriate adsorbents to eliminate the filtration step required by nanoparticles (**Wang et al., 2013; Zhao et al., 2017**). Therefore, a highly efficient material with an ideal removal efficiency is essentially required for exploration and application.

Electrospinning is a flexible method that can create long-length fiber sheets with controlled diameters in the range of hundreds of nanometers for high-tech applications (**Kale et al., 2021**). Additionally, electrospun polymers have been successfully used in orthopedic, anti-bacterial, and wound healing applications, as well as in the removal of organic contaminants, estrogens, heavy metals, and dyes from wastewater (**Chigome et al., 2011; Chigome and Torto, 2011; Kanu et al., 2021, 2020**). Therefore, combining two processes of recycling and organic molecule removal through the effective utilization of electrospun recycled waste CBs proves to be a useful tool in reducing litter and also a great way to treat wastewater. A limited number of works have been conducted with CBs for the removal of

pollutants from wastewater, such as the removal of bisphenol-A and estrogenic hormones (**Alhokbany et al., 2020; Yasir et al., 2022, 2021**). However, the adsorption effectiveness can be enhanced by turning the CBs into spun fibers (**Arroyo et al., 2020**), thereby allowing the fiber surface to be treated with functionalized molecules depending on the target pollutant type (**Balusamy et al., 2020; Foumani et al., 2019; Patel et al., 2019; Sarika and Shankaran, 2016**). The effectiveness of adsorption can be significantly enhanced by this process using nitrogen-rich compounds (**Araga and Sharma, 2019; Qian et al., 2017**). For example, polyaniline ($PANI$) is a conducting and electroactive polymer synthesized by chemical or electrochemical oxidation (**Stejskal et al., 2017; Zhang et al., 2002**) and contains structural units of benzenoid and quinonoid rings connected by nitrogen atoms of amine or imine types through hydrogen bonds and π-π interactions can be used as suitable nitrogen-rich compound (**Ayad et al., 2013; Stejskal, 2020a**). As such, $PANI$ depicts extremely promising features when associated with a composite material for eradicating water pollutants. This improves the interaction capacity of adsorbent by forming complexes with different organic and inorganic substances, leading to enhanced adsorption capacity that decreases the residual concentration of the pollutants (**Stejskal, 2020b**). Combining CBs fibers under ideal conditions with $PANI$ serves as an ideal candidate for the removal of different pollutants. To the best of our knowledge, no such study has been reported in literature where littered waste produced by CBs is reduced and also used in the efficient removal of water pollutants.

In this study, electrospun cellulose acetate from recycled CBs is surface coated via in-situ polymerization with $PANI$ stabilized in a PVA solution for the optimal removal of azo dyes. The fibers were prepared with the least possible diameter to achieve a large surface area for interaction with dye molecules and then further functionalized by coating with $PANI$, thereby creating more sites available for adsorption. The developed material was then explored for its removal efficiency via batch adsorption study, adsorption kinetics, isotherms, and thermodynamics to monitor and evaluate the interaction mechanism involved. In addition, adsorption performance in a combined mix pollutant system and reusability were tested to assess the viability of $CA-PANI$. This study suggests a simple way to remedy the performance of CA nanofibers by applying PANI on the fiber surface. With this suggestion in this study, the interaction with pollutant molecules is increased, and the removal efficiency is enhanced, making $CA-PANI$ suitable for use at an industrial scale.

2. Materials and methods

2.1. Materials

The waste cigarette butts (CBs), independent of producing companies, were gathered in a month from the trash bins situated at the Centre of Polymer Systems, Tomas Bata University in Zlin, Czech Republic. Polypropylene (PP) spun-bond (grammage: 30 g/m^2) was bought from PFNonwovens a.s., Czech Republic. N,N-dimethylformamide (DMF, purity >99.5 %) was obtained from Lach-Ner s.r.o., Czech Republic, while borax (sodium tetra-borate decahydrate), citric acid, acetic acid (purity $=$ 99 %), and formic acid (purity $=$ 98 %) were all acquired from PENTA s.r.o., Czech Republic. Polyethylene oxide (PEO) was bought from Scientific Polymer Products, Inc., New York, USA. Ammonium peroxydisulfate (purity ≥98 %) and rhodamine chloride (RC, purity ≥99 %) were purchased from VWR intl., Czech Republic. Aniline (purity ≥98 %), methyl orange (MO, purity ≥95 %), hydrochloric acid (HCl, 37 % purity), ammonium hydroxide (NH_4OH, 99 % purity), and polyvinyl alcohol (PVA, molecular weight 360 kDa) were obtained from Sigma-Aldrich, Czech Republic.

2.2. Extraction of cellulose acetate (CA)

The extraction of the CA fibers proceeded as follows: a determined amount of CBs was rinsed twice with deionized water to eliminate impurities, followed by oven drying at 80 °C for 6 h. The CBs underwent an extra washing with pure ethanol and dried for 4 h at 40 °C before storage. The extraction process proceeded by preparing a binary solution of acetic acid and formic acid in a ratio of 2:1 and was used to dissolve 8 wt% CBs (32 g). An initial quantity of 400 g dissolved CBs solution was produced and stored for further usage. PEO powder (3 wt% of the mass of CBs (0.96 g)) was poured into the mixture to stabilize and enhance the fibers' structural qualities by obtaining beadles fibers. The mixture was stirred using a mechanical stirrer (Heidolph, RZR 2041) followed by agitation at 450 rpm for 6 h for complete dissolution to obtain a suspension solution of CA fibers.

2.3. Electrospinning of CA fibers and modification with polyaniline

Prior to electrospinning, a separate mixture of borax and citric acid (BC) was prepared in a 1:3 ratio, and then 35 wt% of the BC was dissolved in DMF solution under magnetic agitation for 5 h at 350 rpm. The solution was then added dropwise into the CA suspension solution to adjust the electrical conductivity of the polymeric solution to an optimum of approximately 89 $|\mu$S/cm while maintaining the solution's viscosity at about 0.95 Pa.s. CA spun fibers was fabricated with optimized conditions by utilizing the electrospinning method on a 40 cm wide polypropylene non-woven sheet using the NS Lab 200 S equipment (Elmarco, Czech Republic). The solution spray rate from cords was fixed at 0.34 mL/min at a supplied voltage of 75 kV. The collecting fiber sheet fabric rotated at a speed of 10 cm/min with spaced electrodes 18 cm apart, the room humidity kept below 28 %, and a recorded temperature of 26 $\pm$ 1 °C. Subsequently, the solution characteristics were tuned to create beadles, defect-less, and least-diameter-sized fibers from disposed CBs with an average area mass of 0.865 g/m^2 to produce CA spun nanofibers.

The modification of CA spun nanofibers proceeded via oxidative polymerization of aniline on the fiber surface as previously described (**Yasir et al., 2021; Zaghlol et al., 2020**) with slight modifications. Weighed 0.5 g spun CA nanofibers were immersed in a 50 mL solution containing 4 wt% PVA and 0.1 M aniline dissolved in 1 M HCl solution. The prepared solution was allowed for 2 h, permitting the aniline monomer to adhere to the fibers' surface. An equal amount (50 mL) of a 0.125 M ammonium peroxydisulfate solution was added, and the solution was gently stirred. The combination was then left at room temperature for 24 h to allow the aniline to polymerize in the presence of PVA as the stabilizer to form a coating on the spun fibers. As PANI was formed, the initial solution changed to a dark green or black color. The coated spun fibers were then taken out and repeatedly re-suspended in 0.2 M HCL to remove any remaining unreacted monomers and excess $PANI$. Finally, the sample was washed with distilled water to reach pH 7. The obtained coated samples were denoted $CA-PANI$ and then freeze-dried for further use. By suspending the coated membranes in an excess solution of 1 M NH4OH for 24 h, $CA-PANI$ was further deproto-nated into $CA-dPANI$ **(Humpolicek et al., 2012**). The deprotonated $PANI$ base-coated CA nanofibrous membranes (blue color) were subsequently obtained by filtering the leftover solution, repeatedly washed with acetone and water, and dried at room temperature.

2.4. Characterization methods

Fourier-transformed infrared ($FTIR$) spectroscopy was conducted on a spectrophotometer (Nicolet iS5, Thermo Scientific, USA) equipped with an attenuated total reflection mode (iD5-Ge-ATR) to examine the chemical groups of the electrospun CA, $CA-PANI$, and $CA-dPANI$ fibers. The scan rates were maintained at 64 scans/min, and readings performed between 400 and 4000 cm^{-1} range to acquire the $FTIR$ spectra at 4 cm^{-1} resolution. The microstructure of the uncoated and coated materials was analyzed using a scanning electron microscope (SEM) (SPUR a.s., Czech Republic) working at 10 kV of an accelerating voltage. Prior to analysis, the samples were gold-coated to improve visibility. X-ray diffraction (XRD) analysis was obtained with a Mini Flex™ 600 X-ray diffractometer (Rigaku, Japan) to measure the crystallinity of the as-prepared samples. The foil-filtered radiation source CoK_α ($\lambda = 0.179$ nm) was employed, the voltage was set at 40 kV, the current at 15 mA, scanning range between 0° and 60°, and scanning speed was set at 5°/min. The divergence slit was constantly held at 0.1° throughout the measurement. The thermal degradation and stability of the as-prepared samples were analyzed using a Q500 (TGA) thermogravimetric analyzer (TA Instruments, The USA). The samples were heated from room temperature (25 °C) to 600 °C at a heating rate of 10 °C/min and a flow rate of 40-60 mL/min under a constant N_2 atmosphere. The samples were weighed between 5.0 and 7.0 mg before analysis.

2.5. Adsorption study

Dye adsorption studies were performed to analyze the performance of the prepared materials by investigating the effects of five independent variables: contact duration (0-1440 min), pH of the solution (3 —11), initial concentration of dye solution (1-20 ppm), temperature (25-55 °C), and dosage of nanofibers (5-30 mg). By immersing a certain amount of the uncoated and coated CA membranes into 10 mL of MO or RC dye solution, the solutions were gently agitated at 100 rpm using a controlled temperature water bath shaker to reach adsorption equilibrium. The pH was adjusted for the dye solutions using either 0.2 M $NaOH$ or HCl. The uncoated and coated CA membranes were separated after adsorption, and the solution was then examined using a UV-Vis single-beam spectrophotometer (Model I-290, MA, The USA) at a wavelength of 464 nm for MO and 550 nm for RC dye. The equilibrium adsorption capacity (qe) of the adsorbed dye and percentage removal efficiency ($\%R$) were then calculated using **Eqs**. (**1**) **and** (**2**) (**Saya et al., 2021; Y. Zhou et al., 2014**).

$$q_e = \frac{(C_i - C_e)V}{M} \tag{1}$$

$$\%R = \frac{C_i - C_e}{C_i} \times 100 \tag{2}$$

Where q_e (mg/g) is the capacity of dye adsorbed onto the adsorbent at the equilibrium time, C_i (mg/L) and C_e (mg/L) are the given initial and final concentration of dye in solution, and t is the equilibrium contact time (min). The volume of dye in the experimental solutions and the mass of CA-based membranes are represented by V (L) and M (g), respectively.

To assess the selective adsorption behavior of the various dyes on CA-based membranes, 10 mL of aqueous solution containing the mixed organic dyes (5 mL MO and 5 mL RC) with 20 mg of the adsorbent, 20 mg/L of given initial concentrations of dye, solution pH 7, and a temperature of 25 °C were applied. Agitation was carried out at 100 rpm throughout the experiment, and a 3 mL sample of the solution was taken after 1440 min of adsorption for analysis.

2.6. Adsorption kinetics, isotherm, and thermodynamics

A better understanding of the interaction between the adsorbent material and the dyes depends on the kinetics study during adsorption. **Eqs**. (**3**)-(**5**) were used to fit the observed experimental data of adsorption with the pseudo-1st-order, pseudo-2nd-order, and intraparticle diffusion models.

$$\log(q_e - q_t) = \log q_e - \frac{K_1}{2.303}\, t \tag{3}$$

$$\frac{t}{q_t} = \frac{1}{K_2 q_e^2} + \frac{t}{q} \tag{4}$$

$$q_t = K_3 t^{0.5} + C \tag{5}$$

Where q_e and q_t (mg/g) stand for the adsorption capacities at equilibrium and at any given time (t). The pseudo-1st-order adsorption rate constant, the pseudo-2nd-order adsorption rate constant, and the intraparticle diffusion rate constant are denoted by K_1 (min^{-1}), K_2 (g/ mg min), and K_3 (mg/g $min^{0.5}$), respectively, C (mg/g) represents the boundary layer effect.

The isothermal adsorption models illustrate the theoretical underpinnings of the mechanism by which dyes bind to adsorbent and provide insight into adsorption dynamics. The non-linear expressions of the Langmuir and Freundlich models were studied using **Eqs**. (**6**) and (**7**) (**Erdem et al., 2017; Huang et al., 2018; Mohamed et al., 2018; Y. Zhou et al., 2014**).

$$q_e = \frac{q_m K_L C_e}{1 + K_L C_e} \tag{6}$$

$$q_e = K_F C_e^{\frac{1}{n}} \tag{7}$$

Where the adsorption intensity is denoted by n, K_L (L/mg) as Langmuir constant, K_F (mg/g) (L/mg) as Freundlich constant, and q_m (mg/g) as the maximum adsorption capacity. To better understand how temperature affects the adsorption of MO and RC dyes, the thermodynamic parameters were computed, which include the change in Gibb' s free energy ($\Delta G°$), entropy ($\Delta S°$), and enthalpy ($\Delta H°$). The values were determined from the slope and y-intercept of lnKD versus 1/T (linear Van't Hoff plot) to calculate using **Eqs**. (**8**)-(**10**) (**Erdem et al., 2017; Gholami et al., 2016; Ngwabebhoh et al., 2016**).

$$K_d = \frac{C_s}{C_e} \tag{8}$$

$$\Delta G^{\circ} = -RT\ln K_d \quad (9)$$

$$\ln K_D = -\frac{\Delta H^{o}}{RT} + \frac{\Delta S^{o}}{R} \quad (10)$$

Where the equilibrium dissociation constant is denoted by K_d, which is the solid phase ratio to its solute concentration, R (8.314 J/mol K) represents the universal gas constant value, the concentration of the dye adsorbed is given by C_s (mg/L), and the experimental temperature T (K).

2.7. Reusability test

The reusability of modified prepared materials was evaluated for their performance capacity. After dye adsorption, they were recovered and immersed in 0.5 M aqueous $NaOH$ solution for 2 h to remove the dyes. Next, the $CA - PANI$ was immersed in a 0.1 M aqueous HCl solution repeatedly, followed by washing several times with ethanol/distilled water. Seven cycles of testing the $CA - PANI$ fibers' adsorption-desorption capacity were conducted.

2.8. Statistical analysis

Data are shown as means $\pm$ standard errors of the means obtained from at least three different measurements. The variance (ANOVA) test was carried out on a one-way analysis with a significance of $P < 0.05$ to determine the statistical differences using the software Origin Lab v9.0.

3. Results and discussion

3.1. Fabrication of modified cellulose acetate adsorbent

The spun CA nanofibers from waste CBs was modified by coating the nanofibers with $PANI$. The aniline was chemically and oxidatively polymerized by dissolving the monomer in HCl (1 M) solution at room conditions. The polymerization of aniline on the CA nanofibers was initiated by first immersing the CA in a combined dissolved solution of aniline and PVA, then adding ammonium peroxydisulfate dropwise in the aqueous solution. The reaction mixture is highly exothermic; hence, polymerization is controlled at acidic pH $\approx$ 3 to get an emeraldine form of $PANI$. Once the oxidant was added, the mixture was firmly agitated for 24 h to allow complete polymerization. After polymerization, the green mixture modified on the nanofibers of CA was extracted and washed with distilled H_2O and dilute HCl to remove residual $PANI$. Further addition of NH4OH converted the emeraldine acid form into emeraldine base via deprotonation, as shown in **Fig. 1**.

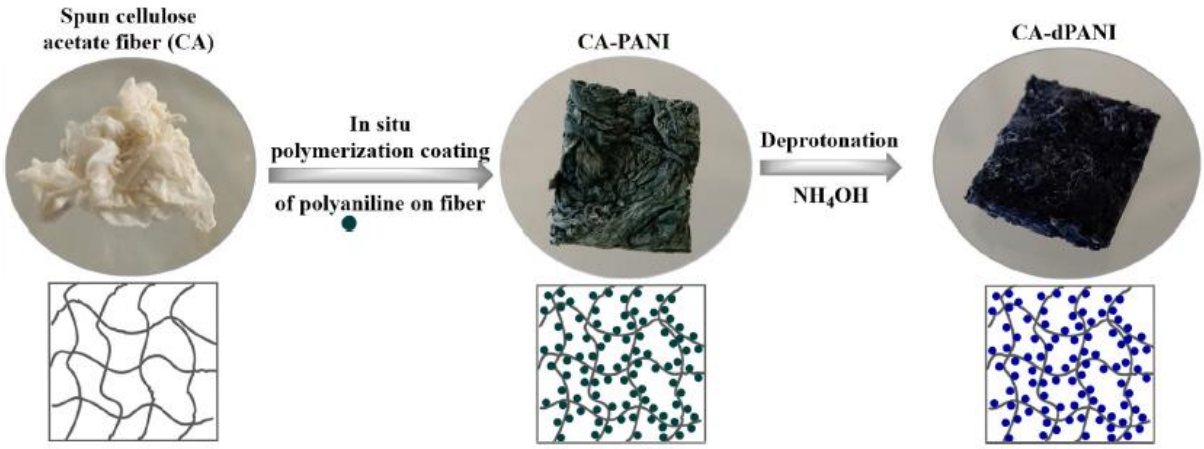

Fig. 1. Illustration of the preparation coating of spun CA fiber forming $CA-PANI$ followed by deprotonation to $CA-dPANI$.

3.2. Characterization techniques

3.2.1. Surface morphology analysis

In contrast to the commercial CA reported in the literature, which has a fiber diameter of 224 $\pm$ 35 nm and a reportedly calculated surface area of 13.6 m^2/g (**Yasir et al., 2021**), **Fig. 2** displays that uniform submicron spun fibers of neat CA (196 $\pm$ 65 nm) produced a relatively thin fiber diameter distribution with negligible beads. This suggests that the CA-spun fibers used in this work may have a greater surface area due to a smaller fiber diameter, resulting in more available active adsorption sites. In addition, due to low intrinsic viscosity, the lowest feasible polymer content in the solution (8 %), and strong electrical conductivity before electrospinning, spun CA fibers have a large surface area produced.

3.2.2. $FTIR$ analysis

Fig. 3a displays the $FTIR$ spectra of neat CA, $CA-PANI$, and $CA-dPANI$ membranes. To see the functional groups present in each sample, the $ATR-FTIR$ characterization was performed. The overlapping stretching vibrations of $N-H$ and OH from CA, PANI, and PVA are indicated by the broadband in the region of 3010-3700 cm^{-1}. Peak intensities for $C=O$ stretching, $C=C$ aromatic bonds, $C-O-C$ anti-symmetric stretching, and $C-O$ bonds could be found at 1740 cm^{-1}, 1370 cm^{-1}, 1234 cm^{-1}, and 1043 cm^{-1}, respectively (**Nasir et al., 2017**). The absorption of the quinone and benzene rings in PANI is responsible for the peaks at approximately 1589 and 1490 cm^{-1} that showed higher intensity for coated CA materials with $PANI$ (**Shahi et al., 2011**). The $C-N$ stretching vibration from CA and $PANI$ is associated with the peaks at 1311 and 1149 cm^{-1}, which also showed enhanced intensity for PANI-coated CA materials. The confined n localized polaron band of coated $PANI$ on CA fibers is responsible for the peak at 834 cm^{-1}, which also displayed higher intensity for the $PANI$-coated samples (**Huang et al., 2016**).

3.2.3. X-ray diffraction analysis

The XRD data (**Fig. 3**b) showed a broad single peak near $2\theta = 21.2°$, indicating that CA-spun fibers are naturally semi-amorphous. According to previously published research, the XRD pattern of cellulose exhibits diffraction peaks at $2\theta = 11.10°$, 21.20°, and 46.40°, which are ascribed to the diffraction planes of 101, 002, and 040, respectively (**Taha et al., 2012**). Due to the acetylation, the diffraction peak at $2\theta = 11.10°$ is associated with the characteristic of CA. The wide-ranged peak concentrated at 21.20° indicates less crystalline cellulose region. An apparent change in the spectrum was observed after the modification of the CA membrane with $PANI$. One can observe the presence of $PANI$ in the CA matrix due to the diffraction peaks in the XRD spectrum of $CA - PANI$ and $CA - dPANI$. Still, the intensities of these peaks were approximately the same but broader than those in the spectrum of neat CA, showing the interaction between CA and $PANI$. Obviously, the crystallinity in the composite membranes arises due to the presence of CA. After the incorporation of $PANI$, the diffraction peaks in the XRD spectrum of the composite membranes broaden due to the semi-crystalline structure of $PANI$. However, no characteristic peak of $PANI$ was observed, depicting that the crystallinity phase of $PANI$ has been overlayed by the crystalline nature of CA with no significant influence on the CA fibers. This result may also be attributed to the strong interfacial interaction between CA and $PANI$ that confines their crystallization. However, the appearance of the new peak at $2\theta = 26.80°$ in the spectrum of $CA - PANI$ is associated with the semi-crystalline nature arising from diffraction planes of benzenoid and quinoid rings of $PANI$ (**Z. Zhou et al., 2014**).

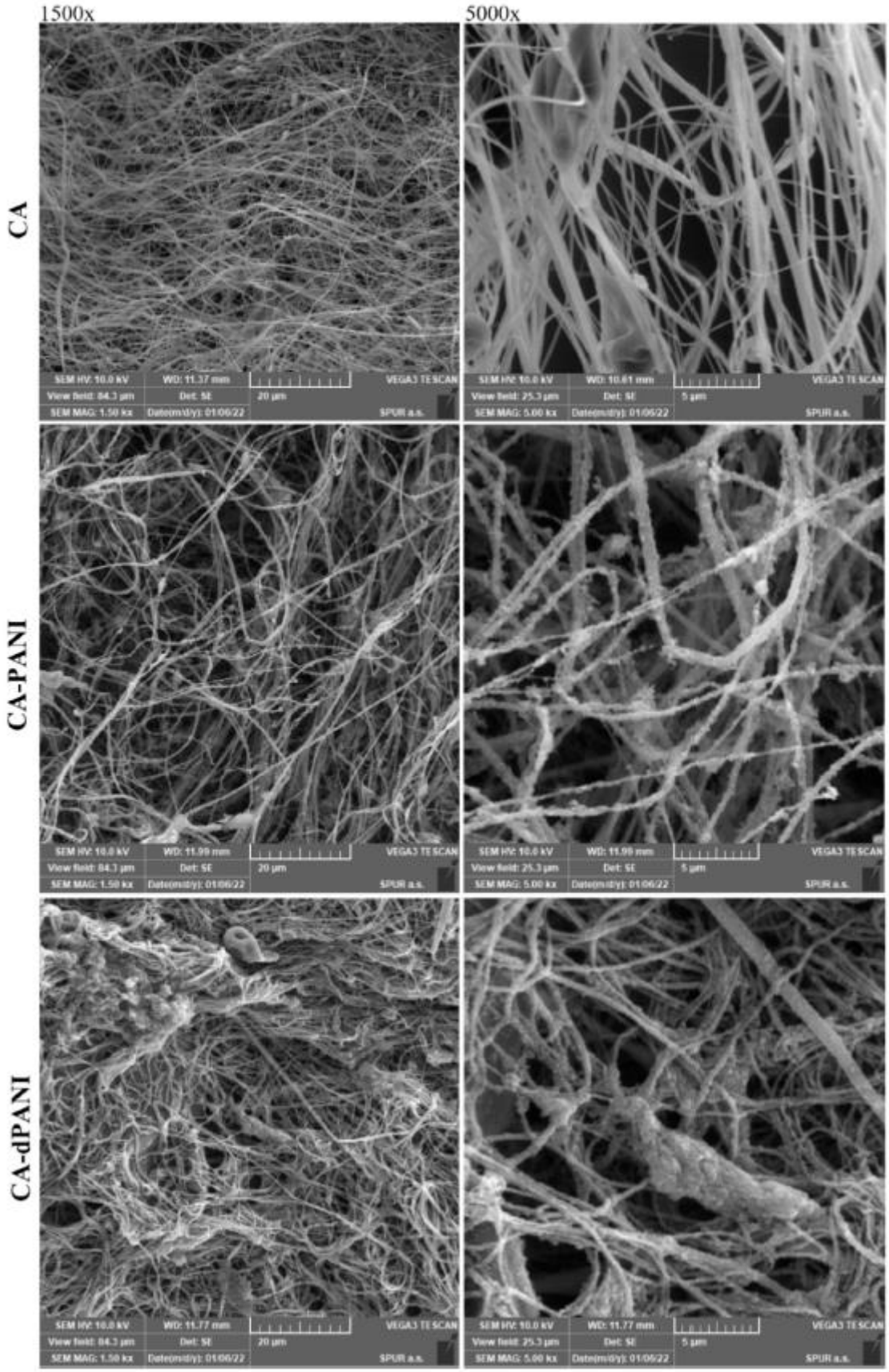

Fig. 2. The SEM images of CA, $CA-PANI$, and $CA-dPANI$

3.2.4. Thermal analysis

The thermal degradation temperature of CA fibers was found to be approximately 356 °C (according to TGA, **Fig. 3**c), which was further enhanced by modifying the fibers with $PANI$ as the peaks shift to the right side (DTGA thermograph, **Fig. 3**d) (**Arroyo et al., 2020**).

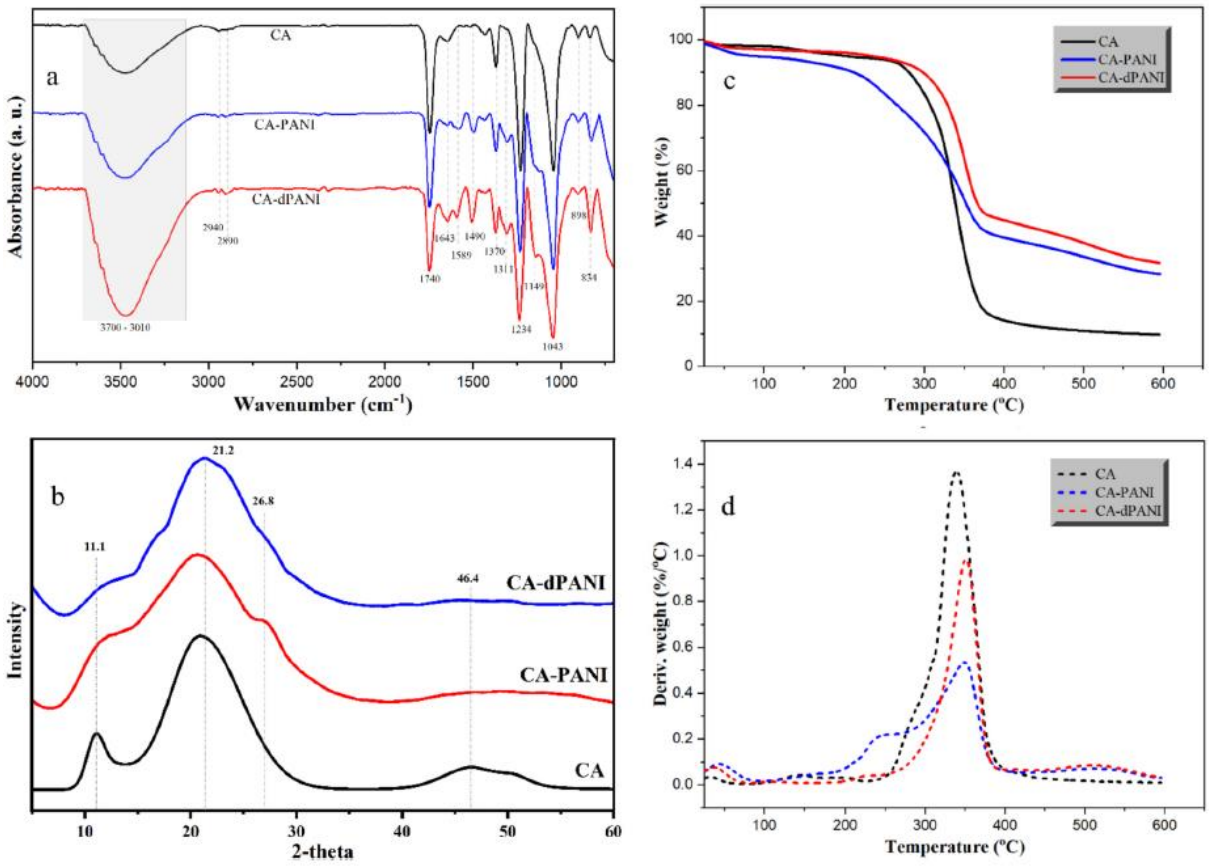

Fig. 3. a) $FT-IR$, b) XRD, c) TGA, and d) $DTGA$ plots of CA, $CA-PANI$, and $CA-dPANI$ spun fibers.

Up to 200 °C, no material degradation was observed. According to our previously reported study, the glass transition temperature (Tg) of CA fibers from waste cigarettes (approximately 180-190 °C by DSC thermogram) stays far over the standard laboratory operating adsorption conditions of temperatures (25-55 °C) (**Yasir et al., 2022**). Furthermore, the degradation of CA starts near the range of 260 °C up to 380 °C. It can also be seen that the wide range of CA fiber degradation is narrowed by modifying with PANI (**Fig. 3**d), which indicates that the PANI coating is highly stable. The initial steady slope may be caused by water evaporation. Thus, CA-spun fibers are thermally stable, and the stability is further enhanced in the case of modified $CA-PANI$ and $CA-dPANI$, indicated by a slight peak shift. As such, these spun fibers would not degrade during application at any operated temperature condition used, for example, during the adsorption process (**Alhokbany et al., 2020; Benavente et al., 2019**).

3.3. Batch adsorption analysis

Conducting polymers, such as PANI, have been extensively used in the removal of organic dyes from the aqueous media by adsorption. However, the combination of polymeric fiber materials with conducting polymers shows potential interest in the design of tunable functional adsorbents. Preliminary tests were conducted for adsorption experiments to evaluate the performance of the

prepared CA, $CA-PANI$, and $CA-dPANI$ adsorbent materials. As observed from **Fig. 4**a and b, the removal performance of the adsorbent for MO and RC dyes was more efficient using $CA-PANI$ with over 90 % and 55 % removal percentages, respectively. This high removal efficiency for $CA-PANI$ was associated with the significant interaction between protonated amine functional groups present in the adsorbent and the dissociated dye molecule species. Compared to CA and $CA-dPANI$, the observed low removal efficiency was attributed to the negatively charged backbone of the materials, leading to the repulsion in interaction with the dye molecules, especially anionic MO dye. As observed from the insert images in **Fig. 4**c and d, the removal of the dyes by the different adsorbents was highly significant using $CA-PANI$ with an almost transparent solution obtained. In contrast, the removal of RC dye appeared average due to the cationic nature of the dissociated dye in the solution. Furthermore, due to its high performance, $CA-PANI$ was selected as the most suitable adsorbent. Therefore, it was used to determine the effect of variation in a single parameter to obtain the optimized parameters.

3.3.1. Effect of contact time

The results in **Fig. 5**a present the relation of equilibrium adsorption capacity and removal efficiency versus contact time for MO and RC dye using $CA-PANI$ spun fibers, respectively. For MO, it can be seen that adsorption capacity reached about 24 mg/g with a gradual increase in a total contact time of over 1440 min, and the removal efficiency of MO dye was achieved at about 99 %. Whereas, for RC dye, the equilibrium adsorption capacity reached saturation in 700 min and then remained constant while the total removal efficiency was nearly 55 %. It is also worth noting that the adsorption of RC was more abrupt in the first 700 min because more adsorption sites were available. Then, the constant adsorption was relatively gradual because of the presence of few sites left to be occupied before saturation.

3.3.2. Effect of solution pH

The results in **Fig. 5**b elucidate the relation of equilibrium adsorption capacity (primary axis) and removal efficiency (secondary axis) vs. solution pH for MO and RC dye using $CA-PANI$ spun fibers, respectively. For MO, the optimum adsorption was observed at pH 7, where the calculated capacity and removal efficiency were found to be 5.37 mg/g and 99 %, respectively. In contrast, a minimum of 4.7 mg/g and 94 % were observed at pH 3. The trend shows decreasing adsorption capacity and removal efficiency at higher basic and acidic conditions. In the case of RC, the trend is quite different. The adsorption capacity and removal efficiency increase from pH 3-11, lowest at pH 3 and highest at pH 11. The highest adsorption capacity was about 3 mg/g, and removal efficiency was around 62 % (chemical interaction is discussed in the adsorption mechanism section).

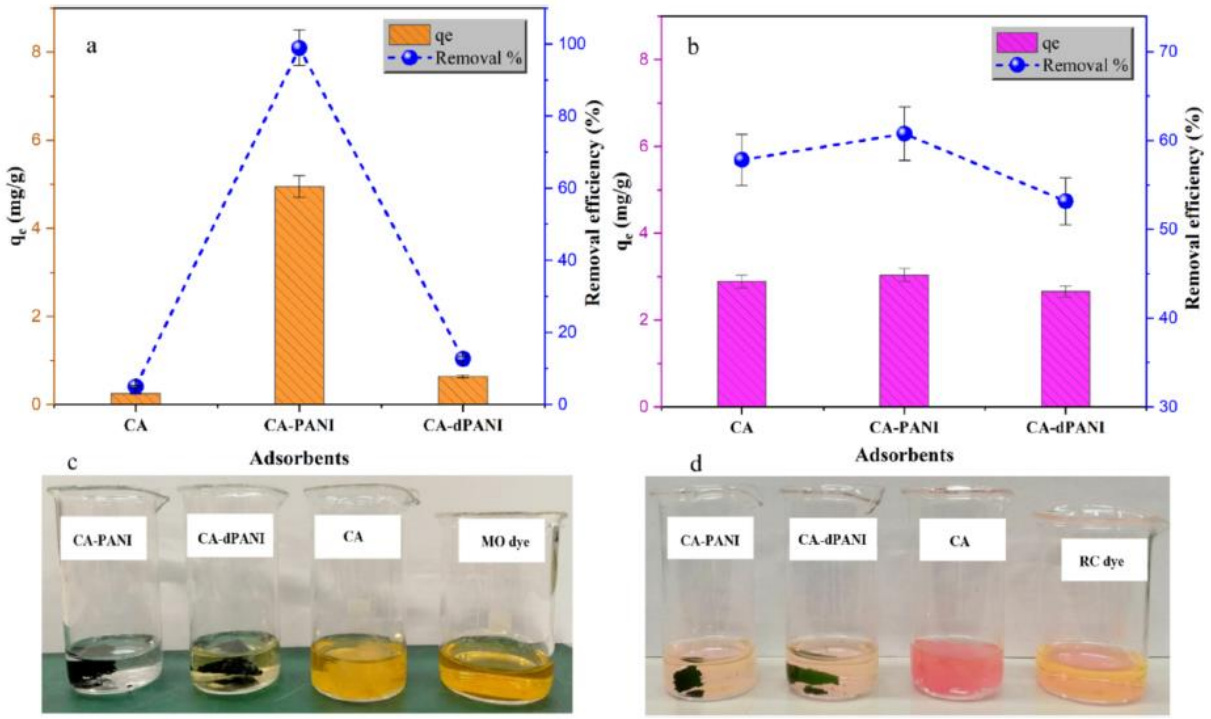

Fig. 4. Adsorption efficiency of the prepared spun and coated CA fibers for a) MO and b) RC dye, and the insert images showing the removal performance of the different adsorbents for c) MO and d) RC dye.

3.3.3. Effect of dye concentration

Fig. 5c elaborates on the relation of equilibrium adsorption capacity and removal efficiency versus initial concentration of dye for MO and RC dye using $CA-PANI$ spun fibers, respectively. A similar trend is seen for both dyes: removal efficiency was reduced. At the same time, the adsorption capacity was increased with the rise in the given initial concentration of dye in the solution from 1 to 20 ppm. For MO dye, at 1 ppm concentration, the efficiency was 100 % and eventually decreased to 89 % at 20 ppm. While for RC, the efficiency dropped from 80 % to 50 % over the same concentration range. At the higher concentration, it is evident that the removal efficiency decreases because the dye entirely fills the available adsorption sites of $CA-PANI$ fibers, and the solution is in excess. In the case of adsorption capacity, the value increases from 0.5 to 9 mg/g for MO dye and from 0.4 to 5.5 mg/g for RC dye when the initial concentration of dye solution was increased from 1 to 20 ppm, respectively.

3.3.4. Effect of adsorbent dosage

Fig. 5d demonstrates the effect on equilibrium adsorption capacity and removal efficiency for MO and RC dye versus adsorbent dosage of $CA-PANI$ spun fibers, respectively. The capacity of adsorption improves from 0.25 to 2.8 mg/g for MO dye and a slight increase from 4.8 to 4.95 mg/g for RC dye, with increasing dosage of nanofibers from 5 to 30 mg, respectively. The rise in the capacity of adsorption is observed because when the amount of $CA-PANI$ spun fibers is increased in the solution, the surface area of $CA-PANI$ spun fibers is increased, which offers more active available sites and interaction for the adsorption of dyes on its surface. Furthermore, the higher nanofiber dosage leads to enhanced removal efficiency of both dyes. The efficiency values rose from 5 % to approximately 60 % for MO and 96 % to over 99 % for RC dye. Overall, the effect of the adsorbent dosage of $CA-PANI$ spun fibers had more impact on the adsorption of MO dye compared to RC dye.

3.3.5. Effect of solution temperature

Temperature is a vital parameter for an adsorption process. A change in the temperature of the adsorption medium can significantly vary the equilibrium adsorption capacity of the adsorbent for a given adsorbate. To study the effect of temperature on the adsorption of MO and RC dyes, solution temperatures were varied from 25 to 55 °C by performing the experiments in a temperature-controlled water bath. **Fig. 5**e depicts the influence of temperature on the equilibrium capacity of adsorption and removal efficiency of $CA - PANI$ spun fibers for MO and RC dyes. As observed, both dyes showed a decreasing trend in removal capacity with increasing temperature, indicating that this process of adsorption is more exothermic. Increasing the temperature decreases the adsorptive forces between the dye molecules and the active sites on the $CA - PANI$ fiber, reducing the amount of dye adsorbed, and thus, adsorption will be more favorable at lower temperatures. The optimum values are reported at 25 C and the lowest at 55 C. It is also noted that the efficiency of MO removal dropped from 99 % to 96.6 %, while for RC, the values decreased from 51 % to 44 % with an increase in temperature. Furthermore, adsorption capacity declined from 4.95 to 4.81 mg/g and 2.55-2.2 mg/g for MO and RC dye, respectively.

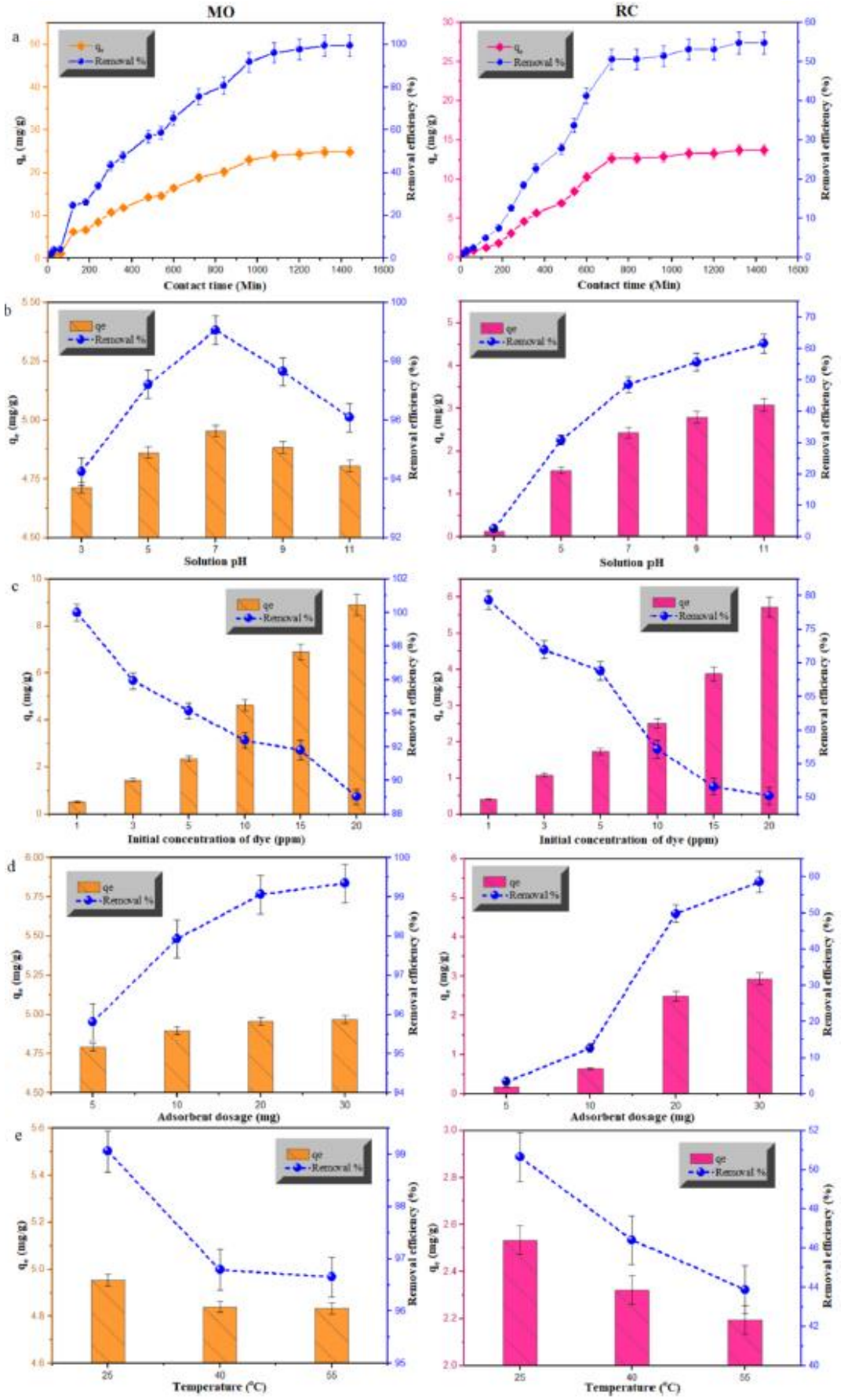

Fig. 5. The influence of a) contact time, b) solution pH, c) initial concentration of dye in solution, d) nanofiber dosage, and e) temperature effect on the adsorption removal of MO and RC dyes by $CA-PANI$ fibers.

3.4. Adsorption mechanism and adsorption kinetics

It is commonly known that an aqueous solution's pH determines how much a dye molecule ionizes. While RC has two amine groups (-NH_2) and a carboxylic group (-$COOH$), MO has a sulfonated group (-SO_3Na). As seen in **Fig. 6**, when the functional groups of the dyes are ionized in aqueous solutions, MO stays in an anionic form, whereas RC changes to a cationic state. At optimum pH 7, $CA-PANI$ introduced into the adsorption solution remains in emeraldine salt form.

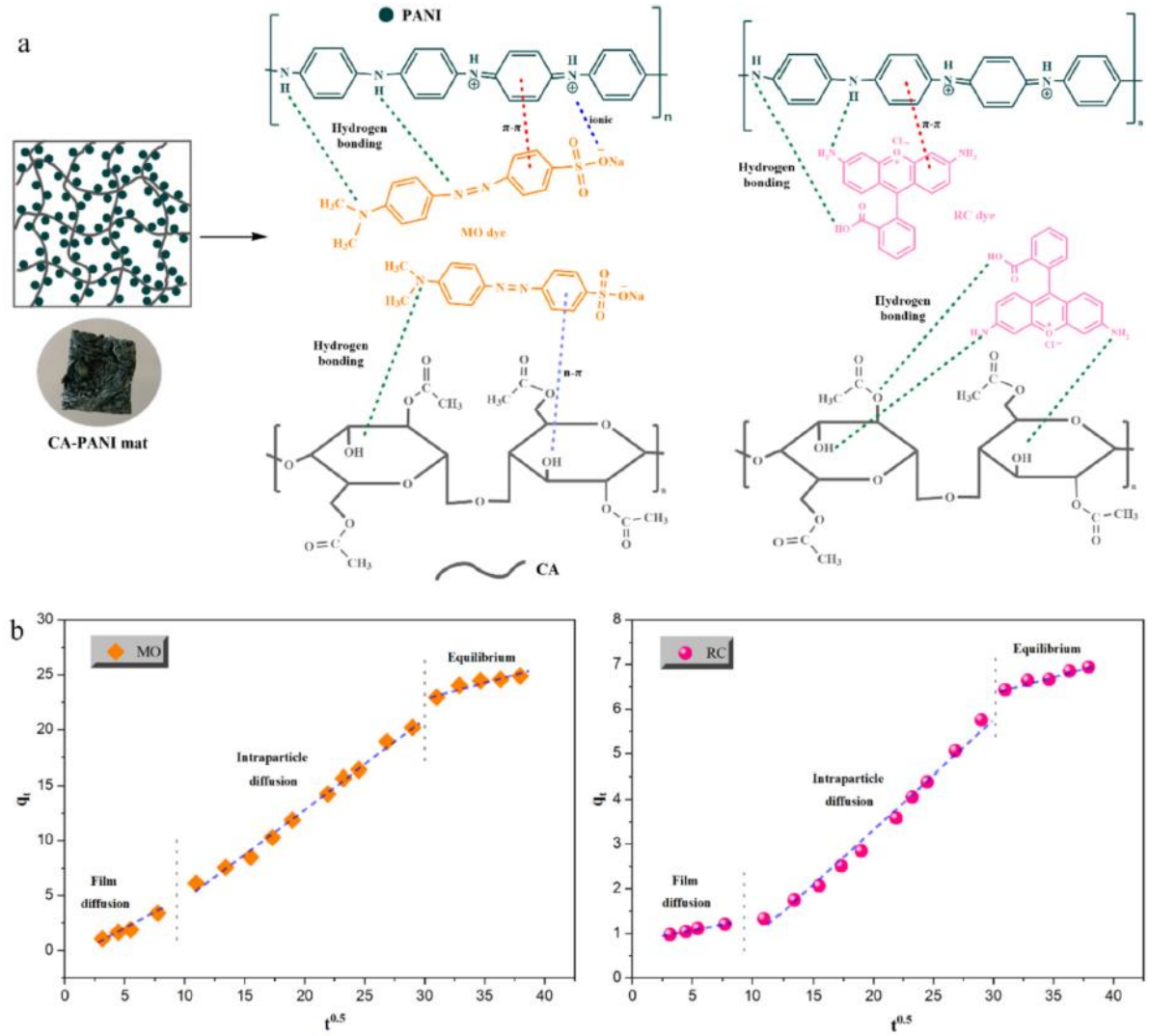

Fig. 6. a) Schematic illustration of the possible interaction mechanism occurring between the MO and RC dye molecules with $CA-PANI$ fiber as adsorbent material. b) The three steps involved in MO and RC dye adsorption mechanism on $CA-PANI$ fiber using the intraparticle diffusion model.

In this form, the adsorbent material is predominantly dominated by -NH and -NH^+ functional groups due to coated $PANI$ on the CA fiber surface. As such, the dissociation of MO dye in this solution produces sulfonated (-SO^3-) groups that ionically interact with the positively charged backbone of CA-PANI (emeraldine salt). While the neutral or negatively charged species of -NH_2 and -$COOH$ present when dissolved in solution weakly interact with the positively charged functional amine groups on $CA-PANI$. On the other hand, the formation of $CA-dPANI$ (emerald base) in basic aqueous solutions inhibits and causes repulsion with the functional groups of the dyes. This lack of chemical and electrostatic interactions with the adsorbent material leads to repulsion due to the formation of

negatively charged species present on the adsorbent and dye molecules. This indicates and confirms that the base form ($CA-dPANI$) adsorption efficiency was significantly low when compared to that of the acid form ($CA-PANI$). This is true when the emeraldine base of PANI is employed in place of the emeraldine salt for the adsorption studies. This suggests that the positively charged backbone of $CA-PANI$, which is typically associated with amine, carboxylic, and hydroxyl groups, provides the potential sites for chemical interactions with the dye molecules. In this study, it can be mentioned that the adsorption process of the dye molecules was predominantly controlled by the combined mechanisms of electrostatic attraction/repulsion and intermolecular hydrogen bonding interactions. Other forces, such as n-n complex interaction between the dye molecules and $CA-PANI$, occurred and was enhanced by the rich phenolic hydroxyls on the surface of $CA-PANI$ (**Stejskal et al., 2023b**, **2023a**).

Three kinetic models (pseudo-1st-order, pseudo-2nd-order, and Weber-Morris intraparticle diffusion model) were used to investigate the experimental data that can best fit to elucidate the ability of adsorption of MO and RC dyes on $CA-PANI$ spun fibers. **Table 1** represents the experimental data values compared to the calculated expected values. It can be interpreted that the pseudo-second-order model shows a firm agreement for MO and RC dyes with the predicted adsorption capacity of 25.653 and 7.145 mg/g, which are quite close to the experimental values of 24.872 and 6.934 mg/g, respectively. Additionally, the values of regression coefficients are also high compared to pseudo-first-order, indicating that both dyes follow pseudo-second-order kinetics. However, the regression coefficients are also high while using the intraparticle diffusion model (**Fig. 6**); the curve is defined in three-step regions, indicating that not only one model solely fits, but more mechanisms are involved in the adsorption process.

Table 1 Parameters involved in Kinetic models for MO and RC dye adsorption using $CAPANÍ$ fibers.

Parameters	MO dye			RC dye		
Pseudo-1st-order model						
q_e, exp (mg/g)	24.872			6.934		
q_e, cal (mg/g)	14.594			3.593		
$K_1 \times 10^{-3}$ (min^{-1})	1.360			1.261		
R^2	0.624			0.614		
χ^2	10.994			10.029		
Pseudo-2nd-order model						
q_e, exp (mg/g)	24.872			6.934		
q_e, cal (mg/g)	25.653			7.145		
$K_2\ 10^{-5}$ (g/mg min)	9.185			34.069		
R^2	0.946			0.896		
χ^2	1.959			3.869		
Intraparticle diffusion model						
	Step 1	Step 2	Step 3	Step 1	Step 2	Step 3
K_3 (mg/g $min^{0.5}$)	0.508	0.817	0.254	0.049	0.248	0.069
C (mg/g)	0.626	3.497	15.386	0.818	1.667	4.288
R^2	0.972	0.993	0.881	0.992	0.987	0.956
χ^2	0.042	0.175	0.088	0.001	0.031	0.002

X^2 = *Redu ced Chi-square.*

Steps 1 and 2 have a steep slope for the adsorption of MO and also illustrate a high regression coefficient of 0.972 and 0.993, which indicates the rate-determining step. However, in step 3, the diffusion rate drops, which is observed by a gentle slope as the adsorption progresses; this could be

due to the low remaining concentration of dye left in the remaining solution. The plausible reason could be the boundary layer effect that might have shadowed the adsorption process in step 3. In comparison, a similar process was observed for RC dye compared to MO in the 2nd and 3rd steps of the adsorption process. At the same time, a low effect of the intraparticle diffusion model is observed in the 1st step, where the pseudo-second-order model was dominant.

3.5. Adsorption thermodynamics and Isotherm model study

Table 2 shows the results obtained from the thermodynamic study. In general, the equilibrium adsorption capacities and removal efficiencies of MO and RC decreased with an increase in temperature (**Fig. 5**e). Here, the values reported in **Table 2** for ΔH and ΔG were determined to be negative.

Table 2 Calculated thermodynamic and isotherm parameters for MO and RC dye adsorption on $CA-PANI$ fiber.

Thermodynamics						
Parameters	*Temperature*					
	MO dye			RC dye		
	298 K	*313 K*	*328 K*	*298 K*	*313 K*	*328 K*
ΔG (kJ/mol)	-11.09	-9.86	-8.62	-0.042	0.327	0.696
ΔH (kJ/mol)	-35.67			-7.38		
ΔS (J/mol K)	-82.48			-24.61		
Isotherm models						
			MO dye	RC dye		
Langmuir model						
Q_{max} (mg/g)			15.601	6.975		
K_L (L/mg)			1.293	0.205		
R_L			0.037–0.436	0.196–0.830		
R^2			0.851	0.692		
χ^2			0.111	0.453		
Freundlich model						
K_F (mg/g)(L/mg)			5.377	1.150		
1/n			0.621	0.796		
R^2			0.979	0.970		
χ^2			0.109	0.135		

X^2 = Reduced Chi-square.

This indicates that the adsorption process for removing MO and RC dyes by $CA-PANI$ spun fibers is exothermic and spontaneous, thus most favorable at low temperatures for maximum output. The values of AG ranged from — 11.09 to — 8.62 kJ/mol and from — 0.042-0.696 for MO and RC dye, respectively. The lower values of MO compared to RC dye depict that MO dye favors a more exothermic nature. The values of AH were below 20 kJ/mol in both dyes, indicating that the dyes are adsorbed on $CA-PANI$ spun fibers by a physical adsorption mechanism. The negative value of AS entropy suggests an overall decrease in the randomness of the solid/solute interface in the solution.

The parameters of the Langmuir and Freundlich equilibriums, as well as the fitting correlation coefficients, are shown in **Table 2**. The Freundlich isotherm proved to best characterize the adsorption process of MO and RC dye based on the correlation coefficients (R^2 and $X^2$2) of two adsorption

isotherms. This shows that the adsorption process, in this case, follows multilayer adsorption on the surface of the nanofiber membrane. The results demonstrated lower values obtained from the Langmuir isotherm model ($R^2 = 0.851$ for MO and 0.692 for RC) as compared to higher R^2 values for Freundlich ($R^2 = 0.979$ for MO and 0.970 for RC) isotherm models (**Table 2**). The maximum Langmuir adsorption capabilities (qm) for the MO and RC dyes were calculated to be 15.60 and 6.97 mg/g, respectively, indicating that the MO dye was better at adsorbing than the RC dye. This can be due to the MO and RC salts' formation of negative and positive species, which increased intermolecular interaction with the $CA-PANI$ adsorbent, which contains positive charge moieties. The dimensionless separation factor (R_L) for MO and RC on $CA-PANI$ was $<$ 0.830, indicating a successful adsorption procedure. On the other hand, it was found that the values of 1/n resulting from the Freundlich isotherm model for the MO and RC dyes, respectively, were 0.621 and 0.796, which are both less than 1, indicating that $CA-PANI$ fiber can serve as a suitable candidate for the adsorption of these azo dyes.

3.6. Adsorption performance of $CA-PANI$ in mixed dye systém

In a mixed dye system, the different dyes' selective adsorption behavior is more intriguing and demanding. A synthetic mixed system comprising the two dyes under investigation was used to gauge the $CA-PANI$ membrane's capacity for selective adsorption. Unexpectedly, MO removal seemed substantially higher than RC, as shown in **Fig. 7**a, and nearly comparable to the single dye adsorption system. This indicates that the co-existence of the cationic RC dye does not affect the uptake of the anionic, even though they might interact with each other via electrostatic attraction. The present experiment was conducted at pH 7, but changing the pH of the dye solution to acid or alkaline may drastically impact the uptake of either dye. That is, the separation of MO and RC in a mixed system as well as the selective adsorption property of $CA-PANI$, may be accomplished simply by altering the solution pH. The fact that the CA-based fibers can be protonated or deprotonated, the pH shift will also have an impact on its characteristics.

3.7. Adsorption-desorption study

Fig. 7a illustrates the relation of removal efficiency (primary axis) and equilibrium adsorption capacity (secondary axis) for MO and RC dye in a mixed solution using $CA-PANI$ spun fibers. It can be seen MO has dominant adsorption removal efficiency and capacity with values $\sim$ 99 % and 5 mg/g, respectively. In the case of RC, the values achieved were 50 % and 2.7 mg/g for removal efficiency and adsorption capacity, respectively. Furthermore, **Fig. 7**b demonstrates the adsorption of MO and RC over seven cycles. It can be seen for MO that the adsorption remained above 82 % after seven cycles for $CA-PANI$ fibers, and there was a negligible drop in efficiency for the first three cycles. In contrast, the percentage adsorption of RC by $CA-PANI$ fibers dropped gradually from about 59 % in the first cycle to 30 % after seven regeneration cycles.

To determine the effectiveness of removing cationic and anionic dyes from the water, the produced $CA-PANI$ membrane's adsorption performance was compared to that of other previously researched adsorbents. The produced $CA-PANI$ fiber material in the present investigation has good adsorption performance and the potential to remove organic pollutant dyes from contaminated water, as shown in **Table 3**. The other reported adsorbents, which are nanoparticles, possess relatively higher adsorption capacity owing to their higher surface areas than the electrospun $CA-PANI$ fibers.

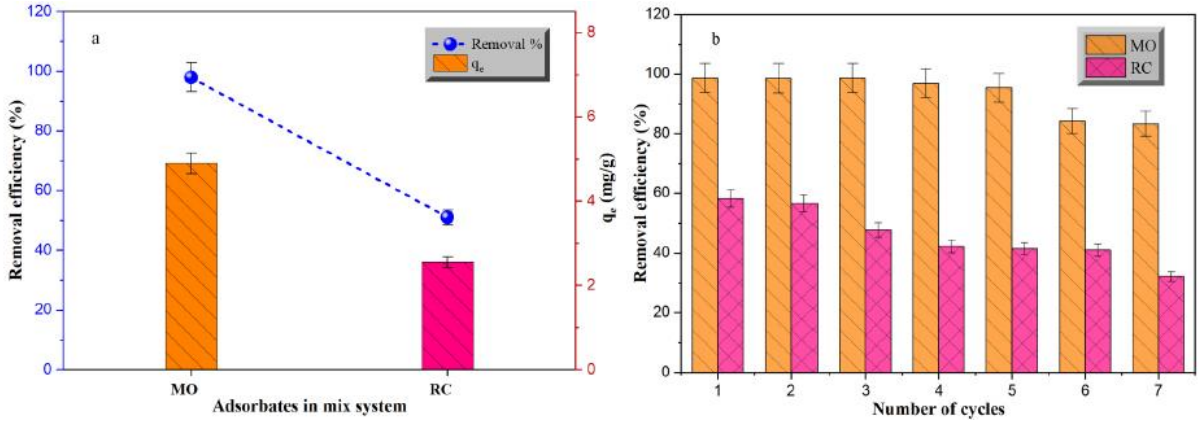

Fig. 7. a) Selection adsorption efficiency of $CA-PANI$ for the MO and RC dye in a mixed adsorbate system, and b) Reusability of $CA-PANI$ by an adsorption-desorption process for the uptake of MO and RC dye.

4. Conclusions

An efficient and easy-to-use CA-based adsorbent extracted from waste cigarette butts was modified with $PANI$ via chemical oxidation polymerization. The fibers rapidly adsorb different azo dyes (MO and RC) in aqueous phase. The strong interaction between the hydroxyl, carboxylic, and amine groups on pristine polymers endowed $CA-PANI$ with good stability and high removal performance by facilitating the binding of MO and RC dyes on the adsorbent. SEM analysis depicted good adhesion of $PANI$-stabilized particles on the nanofibers of CA. At a given dye concentration of 10 mg/L, pH of 7, nanofiber dosage of 20 mg, temperature of 25 °C, and an equilibrium contact time of 1440 min, maximum removal efficiencies of 99 % and 55 % and capacities of 24.87 mg/g and 6.93 mg/g for MO and RC dye were attained, respectively. The most accurate descriptions of the adsorption process were observed with pseudo-2nd-order and Freundlich models. Additionally, kinetics investigations revealed that the surface reaction between the dyes and $CA-PANI$ controlled the rate-determining step of adsorption for MO and RC. The CA-spun fibers were demonstrated to be a technically feasible development as they can be reusable for several adsorption-desorption cycles with acceptable adsorption capacities for MO and RC. Furthermore, the effects of a mixed dye system further demonstrated that hydrogen bonding and electrostatic attraction were the primary interactions for efficiently removing the dyes. Moreover, the thermodynamics result indicated the spontaneous and exothermic nature of the adsorption process. This research offers a new method for enhancing the adsorption efficiency of CA-based materials modified with richer polymers like $PANI$, which could find use in practical wastewater filtration processes.

Table 3 Comparison of the maximum removal efficiency of $CA - PANI$ with other fiber-based adsorbents found in the literature for MO and RC adsorption.

Adsorbents	Dye	q_e (mg/g)	Optimal adsorption conditions	Reference
Graphene oxide/ polydopamine	RC	26.34	pH 4.0, 25 °C, 10 mg/L, 180 min	(Wang et al., 2021)
MOF/bacterial cellulose nanocomposites	RC	2.77	pH 7.0, 25 °C, 10 mg/L, 180 mg and 1440 min	(Ashour et al., 2020)
Impregnated Polymeric Dowex 5WX8 Resin	RC	43.47	pH 3.6, 25 °C, 100 mg/L, 300 mg and 30 min	(Ali Khan et al., 2020)
CA-PANI	**RC**	**6.93**	**pH 7.0, 25 °C, 10 mg/L, 20 mg and 1440 min**	**This study**
Activated carbon PANI	MO	195.52	pH 6.0, 25 °C, 100 mg/L, 10 mg and 120 min	(Bekhoukh et al., 2022)
BPPO-based anion exchange membrane	MO	18.82	pH 8.0, 50 °C, 100 mg/L, 10 mg and 2800 min	(Khan et al., 2022)
Modified fly ash-based geopolymer	MO	19.23	pH 2.0, 25 °C, 50 mg/L, 200 mg and 120 min	(Purbasari et al., 2023)
Amino-crosslinked hypromellose	MO	15.56	pH 6.0, 35 °C, 50 mg/L, 180 mg and 30 min	(Qu et al., 2020)
CA-PANI	**MO**	**24.87**	**pH 7.0, 25 °C, 10 mg/L, 20 mg and 1440 min**	**This study**

References

Alhokbany, N.S., Naushad, M., Kumar, V., Al hatim, S., Alshehri, S.M., Ahamad, T., 2020. Self-nitrogen doped carbons aerogel derived from waste cigarette butts (cellulose acetate) for the adsorption of BPA: kinetics and adsorption mechanisms. J. King Saud. Univ. Sci. 32, 3351-3358. **https://doi.org/10.1016/jjksus.2020.09.021**.

Ali Khan, M., Momina, Siddiqui, M.R., Otero, M., Alshareef, S.A., Rafatullah, M., 2020. Removal of rhodamine B from Water Using A Solvent Impregnated Polymeric Dowex 5WX8 resin: statistical optimization and batch adsorption studies. Polymers. **https:// doi.org/10.3390/polym12020500**.

Araga, R., Sharma, C.S., 2019. Amine functionalized electrospun cellulose nanofibers for fluoride adsorption from drinking water. J. Polym. Environ. **https://doi.org/10.1007/s10924-019-01394-2**.

Arroyo, F.D., Castro-Guerrero, C.F., Leon-Silva, U., 2020. Thin films of cellulose acetate nanofibers from cigarette butt waste. Prog. Rubber Plast. Recycl. Technol. 36, 3-17. **https://doi.org/10.1177/1477760619895024**.

Ashour, R.M., Abdel-Magied, A.F., Wu, Q., Olsson, R.T., Forsberg, K., 2020. Green synthesis of metal-organic framework bacterial cellulose nanocomposites for separation applications. Polymers. **https://doi.org/10.3390/polym12051104**.

Ayad, M., El-Hefnawy, G., Zaghlol, S., 2013. Facile synthesis of polyaniline nanoparticles; its adsorption behavior. Chem. Eng. J. **https://doi.org/10.1016/). cej.2012.11.099**.

Balusamy, B., Senthamizhan, A., Uyar, T., 2020. Functionalized electrospun nanofibers as a versatile platform for colorimetric detection of heavy metal ions in water: a review. Materials. **https://doi.org/10.3390/ma13102421**.

Bekhoukh, A., Moulefera, I., Zeggai, F.Z., Benyoucef, A., Bachari, K., 2022. Anionic methyl orange removal from aqueous solutions by activated carbon reinforced conducting polyaniline as adsorbent: synthesis, characterization, adsorption behavior, regeneration and kinetics study. J. Polym. Environ. 30, 886-895. **https:// doi.org/10.1007/s10924-021-02248-6**.

Benavente, M.J., Caballero, M.J.A., Silvero, G., López-Coca, I., Escobar, V.G., 2019. Cellulose acetate recovery from cigarette butts. Proceedings 2, 1447. **https://doi. org/10.3390/proceedings2201447**.

Bilge, S., Bakirhan, N.K., Osman Donar, Y., Sinag, A., Ozkan, S.A., 2019. Turning toxic cigarette butt waste into the sensor material for the sensitive determination of antihypertensive drug trandolapril from its dosage form and biological samples. Sens. Actuators B Chem. 296 **https://doi.org/10.1016Zj.snb.2019.126626**.

Carvalho, R.V., Isecke, B.G., Carvalho, E., Teran, F.J.C., 2017. Photocatalytic oxidation of 17 - Ethinylestradiol by UV-activated TiO2 in batch and continuous-flow reactor. J. Chem. Eng. Mater. Sci. 8, 10-16. **https://doi.org/10.5897/jcems2017.0293**.

Castellanos, R.M., Bassin, J.P., Bila, D.M., Dezotti, M., 2021. Biodegradation of natural and synthetic endocrine-disrupting chemicals by aerobic granular sludge reactor: evaluating estrogenic activity and estrogens fate. Environ. Pollut. 274, 116551 **https://doi.org/10.1016/j.envpol.2021.116551**.

Chigome, S., Darko, G., Torto, N., 2011. Electrospun nanofibers as sorbent material for solid phase extraction. Analyst. **https://doi.org/10.1039/c1an15228a**.

Chigome, S., Torto, N., 2011. A review of opportunities for electrospun nanofibers in analytical chemistry. Anal. Chim. Acta. **https://doi.org/10.1016/j.aca.2011.08.021**.

Erdem, A., Ngwabebhoh, F.A., £etinta§, S., Bingol, D., Yildiz, U., 2017. Fabrication and characterization of novel macroporous Jeffamine/diamino hexane cryogels for enhanced Cu(II) metal uptake: optimization, isotherms, kinetics and thermodynamic studies. Chem. Eng. Res. Des. 117, 122-138. **https://doi.org/10.1016/j. cherd.2016.10.010**.

Foumani, M.M., Khorshidi, A., Shojaei, A.F., 2019. PolyethyleneiminE Nanofibers Functionalized with Tetradentate Schiff Base Complexes of Dioxomolybdenum(VI) as efficient catalysts for epoxidation of alkenes. ChemistrySelect. **https://doi.org/ 10.1002/slct.201803047**.

Gao, X., Kang, S., Xiong, R., Chen, M., 2020. Environment-friendly removal methods for endocrine disrupting chemicals. Sustainability 12, 7615. **https://doi.org/10.3390/ su12187615**.

Gholami, M., Vardini, M.T., Mahdavinia, G.R., 2016. Investigation of the effect of magnetic particles on the Crystal Violet adsorption onto a novel nanocomposite based on K-carrageenan-g-poly(methacrylic acid). Carbohydr. Polym. 136, 772-781. **https://doi.org/10.1016/j.carbpol.2015.09.044**.

Hemamalini, T., Karunakaran, S.A., Siva Elango, M.K., Senthil Ram, T., Giri Dev, V.R., 2019. Regeneration of cellulose acetate nanofibrous mat from discarded cigarette butts. Indian J. Fibre Text. Res. 44, 248-252.

Hristovski, K.D., Nguyen, H., Westerhoff, P.K., 2009. Removal of arsenate and 17a-ethinyl estradiol (EE2) by iron (hydr)oxide modified activated carbon fibers. J. Environ. Sci. Health Part A Toxic. Hazard. Subst. Environ. Eng. 44, 354-361. **https://doi.org/10.1080/10934520802659695**.

Huang, H., Yao, J., Li, L., Zhu, F., Liu, Z., Zeng, X., Yu, X., Huang, Z., 2016. Reinforced polyaniline/polyvinyl alcohol conducting hydrogel from a freezing-thawing method as self-supported electrode for supercapacitors. J. Mater. Sci. **https://doi.org/ 10.1007/s10853-016-0137-8**.

Huang, X., Zhan, X., Wen, C., Xu, F., Luo, L., 2018. Amino-functionalized magnetic bacterial cellulose/activated carbon composite for Pb2+ and methyl orange sorption from aqueous solution. J. Mater. Sci. Technol. 34, 855-863. **https://doi.org/ 10.1016/j.jmst.2017.03.013**.

Humpolicek, P., Kasparkova, V., Saha, P., Stejskal, J., 2012. Biocompatibility of polyaniline. Synth. Met. **https://doi.org/10.1016/j.synthmet.2012.02.024**.

Jin, X., Hu, J.Y., Tint, M.L., Ong, S.L., Biryulin, Y., Polotskaya, G., 2007. Estrogenic compounds removal by fullerene-containing membranes. Desalination 214, 83-90. **https://doi.org/10.1016/j.desal.2006.10.019**.

Kale, S.M., Kirange, P.M., Kale, T.V., Jee Kanu, N., Gupta, E., Chavan, S.S., Kumar Vates, U., Kumar Singh, G., 2021. Synthesis of ultrathin ZnO, nylon-6,6 and carbon nanofibers using electrospinning method for novel applications. Mater. Today Proc. 47, 3186-3189. **https://doi.org/10.1016/j.matpr.2021.06.289**.

Kanu, N., Gupta, E., Sutar, V., Singh, G., Vates, U., 2021. An insight into biofunctional curcumin/gelatin nanofibers. Nanofibers. **https://doi.org/10.5772/ intechopen.97113**.

Kanu, N.J., Gupta, E., Vates, U.K., Singh, G.K., 2020. Electrospinning process parameters optimization for biofunctional curcumin/gelatin nanofibers. Mater. Res. Express 7, 0-27. **https://doi.org/10.1088/2053-1591/ab7f60**.

Khan, M.I., Shanableh, A., Elboughdiri, N., Lashari, M.H., Manzoor, S., Shahida, S., Farooq, N., Bouazzi, Y., Rejeb, S., Elleuch, Z., Kriaa, K., ur Rehman, A., 2022. Adsorption of methyl orange from an aqueous solution onto a BPPO-based anion exchange membrane. ACS Omega 7, 26788-26799. **https://doi.org/10.1021/ acsomega.2c03148**.

Kiran Kumar, A., Venkata Mohan, S., 2012. Removal of natural and synthetic endocrine disrupting estrogens by multi-walled carbon nanotubes (MWCNT) as adsorbent: kinetic and mechanistic evaluation. Sep. Purif. Technol. 87, 22-30. **https://doi.org/ 10.1016/j.seppur.2011.11.015**.

Křesinová, Z., Linhartová, L., Filipová, A., Ezechiáš, M., Mašín, P., Cajthaml, T., 2018. Biodegradation of endocrine disruptors in urban wastewater using Pleurotus ostreatus bioreactor. New Biotechnol. 43, 53-61. **https://doi.org/10.1016/j. nbt.2017.05.004**.

Krupadam, R.J., Sridevi, P., Sakunthala, S., 2011. Removal of endocrine disrupting chemicals from contaminated industrial groundwater using chitin as a biosorbent. J. Chem. Technol. Biotechnol. 86, 367-374. **https://doi.org/10.1002/jctb.2525**.

Kumar, A.K., Mohan, S.V., 2011. Endocrine disruptive synthetic estrogen (17a-ethynylestradiol) removal from aqueous phase through batch and column sorption studies: mechanistic and kinetic analysis. Desalination 276, 66-74. **https://doi.org/ 10.1016/j.desal.2011.03.022**.

Kumar, A.K., Mohan, S.V., Sarma, P.N., 2009. Sorptive removal of endocrine-disruptive compound (estriol, E3) from aqueous phase by batch and column studies: kinetic and mechanistic evaluation. J. Hazard. Mater. 164, 820-828. **https://doi.org/10.1016/j. jhazmat.2008.08.075**.

Lu, T., Liang, H., Cao, W., Deng, Y., Qu, Q., Ma, W., Xiong, R., Huang, C., 2022. Blow-spun nanofibrous composite Self-cleaning membrane for enhanced purification of oily wastewater. J. Colloid Interface Sci. 608, 2860-2869. **https://doi.org/10.1016/ j.jcis.2021.11.017**.

Ma, W., Jiang, Z., Lu, T., Xiong, R., Huang, C., 2022. Lightweight, elastic and superhydrophobic multifunctional nanofibrous aerogel for self-cleaning, oil/water separation and pressure sensing. Chem. Eng. J. 430, 132989 **https://doi.org/ 10.1016/j.cej.2021.132989**.

Mohamed, R.R., Abu Elella, M.H., Sabaa, M.W., Saad, G.R., 2018. Synthesis of an efficient adsorbent hydrogel based on biodegradable polymers for removing crystal violet dye from aqueous solution. Cellulose 25, 6513-6529. **https://doi.org/ 10.1007/s10570-018-2014-x**.

Montalvão, M.F., Chagas, T.Q., da Silva Alvarez, T.G., Mesak, C., da Costa Araújo, A.P., Gomes, A.R., de Andrade Vieira, J.E., Malafaia, G., 2019. How leachates from wasted cigarette butts influence aquatic life? A case study on freshwater mussel Anodontites trapesiali. Sci. Total Environ. 689, 381-389. **https://doi.org/10.1016/j. scitotenv.2019.06.385**.

Muhammad, Y., Milan, M., Tomas, S., Hassan, A., Michal, U., Jan, A., Michal, M., Ivo, K., 2022. ZnO nanowires and nanorods based ZnO/WO3/Pt heterojunction for efficient photocatalytic degradation of Estriol (E3) hormone. Mater. Lett. 319, 132291 **https://doi.org/10.1016/j.matlet.2022.132291**.

Nasir, M., Subhan, A., Prihandoko, B., Lestariningsih, T., 2017. Nanostructure and property of electrospun SiO2-cellulose acetate nanofiber composite by electrospinning. Energy Procedia 107, 227-231. **https://doi.org/10.1016/j. egypro.2016.12.133**.

Naz, M., Rafiq, A., Ikram, M., Haider, A., Ahmad, S.O.A., Haider, J., Naz, S., 2021. Elimination of dyes by catalytic reduction in the absence of light: a review. J. Mater. Sci. 56, 15572-15608. **https://doi.org/10.1007/s10853-021-06279-1**.

Ngwabebhoh, F.A., Gazi, M., Oladipo, A.A., 2016. Adsorptive removal of multi-azo dye from aqueous phase using a semi-IPN superabsorbent chitosan-starch hydrogel. Chem. Eng. Res. Des. 112, 274-288. **https://doi.org/10.1016/j.cherd.2016.06.023**.

Pan, B., Lin, D., Mashayekhi, H., Xing, B., 2008. Adsorption and hysteresis of bisphenol A and 17a-ethinyl estradiol on carbon nanomaterials. Environ. Sci. Technol. 42, 5480-5485. **https://doi.org/10.1021/es8001184**.

Patel, S., Konar, M., Sahoo, H., Hota, G., 2019. Surface functionalization of electrospun PAN nanofibers with ZnO-Ag heterostructure nanoparticles: synthesis and antibacterial study. Nanotechnology. **https://doi.org/10.1088/1361-6528/ab045d**.

Purbasari, A., Ariyanti, D., Fitriani, E., 2023. Adsorption of methyl orange dye by modified fly ash-based geopolymer - characterization, performance, kinetics and isotherm studies. J. Ecol. Eng. 24, 90-98. **https://doi.org/10.12911/22998993/ 157541**.

Qian, L., Li, X., Qi, F., Li, J., Lu, L., Xu, Q., 2017. An amino-functionalized grooved nanofiber mat for solid-phase extraction of phenolic pollutants. Microchim. Acta. https://doi.org/10.1007/s00604-017-2313-1.

Qu, W., He, D., Huang, H., Guo, Y., Tang, Y., Song, R.-J., 2020. Characterization of amino-crosslinked hypromellose and its adsorption characteristics for methyl orange from water. J. Mater. Sci. 55, 7268-7282. **https://doi.org/10.1007/s10853-020-04517-6**.

Rafiq, A., Ikram, M., Ali, S., Niaz, F., Khan, M., Khan, Q., Maqbool, M., 2021. Photocatalytic degradation of dyes using semiconductor photocatalysts to clean industrial water pollution. J. Ind. Eng. Chem. 97, 111-128. **https://doi.org/ 10.1016/j.jiec.2021.02.017**.

Rebischung, F., Chabot, L., Biaudet, H., Pandard, P., 2018. Cigarette butts: a small but hazardous waste, according to European regulation. Waste Manag 82, 9-14. **https:// doi.org/10.1016/j.wasman.2018.09.038**.

Saleh, T.A., 2021a. Carbon nanotube-incorporated alumina as a support for MoNi catalysts for the efficient hydrodesulfurization of thiophenes. Chem. Eng. J. 404, 126987 **https://doi.org/10.1016/j.cej.2020.126987**.

Saleh, T.A., 2021b. Protocols for synthesis of nanomaterials, polymers, and green materials as adsorbents for water treatment technologies. Environ. Technol. Innov. 24, 101821 **https://doi.org/10.1016/j.eti.2021.101821**.

Sarika, R., Shankaran, D.R., 2016. Synthesis and characterization of curcumin nanoparticles loaded nanofibers for lead ion detection. Sens. Lett. **https://doi.org/ 10.1166/sl.2016.3707**.

Saya, L., Malik, V., Singh, A., Singh, S., Gambhir, G., Singh, W.R., Chandra, R., Hooda, S., 2021. Guar gum based nanocomposites: role in water purification through efficient removal of dyes and metal ions. Carbohydr. Polym. 261, 117851 **https://doi.org/ 10.1016/j.carbpol.2021.117851**.

Shahi, M., Moghimi, A., Naderizadeh, B., Maddah, B., 2011. Electrospun PVA-PANI and PVA-PANI-AgNO3 composite nanofibers. Sci. Iran. **https://doi.org/10.1016/j. scient.2011.08.013**.

Shen, Feiyue, Tian, D., Yang, G., Deng, S., Shen, Fei, He, J., Zhu, Y., Huang, C., Hu, J., 2020. Deacetylation processing of waste cigarette butts for high-titer bioethanol production toward a clean recycling process. ACS Sustain. Chem. Eng. 8, 11253-11262. **https://doi.org/10.1021/acssuschemeng.0c03979**.

Stejskal, J., 2020a. Interaction of conducting polymers, polyaniline and polypyrrole, with organic dyes: polymer morphology control, dye adsorption and photocatalytic decomposition. Chem. Pap. **https://doi.org/10.1007/s11696-019-00982-9**.

Stejskal, J., 2020b. Conducting polymers are not just conducting: a perspective for emerging technology. Polym. Int. **https://doi.org/10.1002/pi.5947**.

Stejskal, J., Bober, P., Trchová, M., Kovalcik, A., Hodan, J., Hromádková, J., Prokes, J., 2017. Polyaniline cryogels supported with poly(vinyl alcohol): soft and conducting. Macromolecules. **https://doi.org/10.1021/acs.macromol.6b02526**.

Stejskal, J., Ngwabebhoh, F.A., Sáha, T., Prokes, J., 2023a. Coating of carbonized leather waste with the conducting polymer polyaniline: bicontinuous composites for dye adsorption. Coatings. **https://doi.org/10.3390/coatings13081419**.

Stejskal, J., Ngwabebhoh, F.A., Trchova, M., Prokes, J., 2023b. Carbonized leather waste with deposited polypyrrole nanotubes: conductivity and dye adsorption. Nanomaterials. **https://doi.org/10.3390/nano13202794**.

Taha, A.A., Wu, Y. na, Wang, H., Li, F., 2012. Preparation and application of functionalized cellulose acetate/silica composite nanofibrous membrane via electrospinning for Cr(VI) ion removal from aqueous solution. J. Environ. Manag. 112, 10-16. **https://doi.org/10.1016/j.jenvman.2012.05.031**.

Torkashvand, J., Farzadkia, M., 2019. A systematic review on cigarette butt management as a hazardous waste and prevalent litter: control and recycling. Environ. Sci. Pollut. Res. **https://doi.org/10.1007/s11356-019-04250-x**.

Torkashvand, J., Farzadkia, M., Sobhi, H.R., Esrafili, A., 2020. Littered cigarette butt as a well-known hazardous waste: a comprehensive systematic review. J. Hazard. Mater. 383, 121242 **https://doi.org/10.1016/j.jhazmat.2019.121242**.

Wang, J., Pan, K., Giannelis, E.P., Cao, B., 2013. Polyacrylonitrile/polyaniline core/shell nanofiber mat for removal of hexavalent chromium from aqueous solution: mechanism and applications. RSC Adv. 3, 8978-8987. **https://doi.org/10.1039/ c3ra40616d**.

Wang, X., Guo, Y., Jia, Z., Ma, H., Liu, C., Liu, Z., Shi, Q., Ren, B., Li, L., Zhang, X., Hu, Y., 2021. Fabrication of graphene oxide/polydopamine adsorptive membrane by stepwise in-situ growth for removal of rhodamine B from water. Desalination 516, 115220. **https://doi.org/10.1016/j.desal.2021.115220**.

Wei, X., Li, J., Liu, Z., Yang, X., Naraginti, S., Xu, X., Wang, X., 2018. Visible light photocatalytic mineralization of 17a-ethinyl estradiol (EE2) and hydrogen evolution over silver and strontium modified TiO 2 nanoparticles: mechanisms and phytotoxicity assessment. RSC Adv. 8, 4329-4339. **https://doi.org/10.1039/ C7RA12638G**.

Yasir, M., Sopík, T., Lovecká, L., Kimmer, D., Sedlank, V., 2021. The adsorption, kinetics, and interaction mechanisms of various types of estrogen on electrospun polymeric nanofiber membranes. Nanotechnology 33, 75702. **https://doi.org/10.1088/1361-6528/ac357b**.

Yasir, M., Sopik, T., Patwa, R., Kimmer, D., Sedlarik, V., 2022. Adsorption of estrogenic hormones in aqueous solution using electrospun nanofibers from waste cigarette butts: kinetics, mechanism, and reusability. Express Polym. Lett. 16, 624-648.

Zaghlol, S., Amer, W.A., Shaaban, M.H., Ayad, M.M., Bober, P., Stejskal, J., 2020. Conducting macroporous polyaniline/poly(vinyl alcohol) aerogels for the removal of chromium(VI) from aqueous media. Chem. Pap. 74, 3183-3193. **https://doi.org/ 10.1007/s11696-020-01151-z**.

Zhang, Y., Zhou, J.L., 2005. Removal of estrone and 17p-estradiol from water by adsorption. Water Res. 3991-4003. **https://doi.org/10.1016/j.watres.2005.07.019**.

Zhang, Z., Wei, Z., Wan, M., 2002. Nanostructures of polyaniline doped with inorganic acids. Macromolecules. **https://doi.org/10.1021/ma020199v**.

Zhao, J., Lu, Z., He, X., Zhang, X., Li, Q., Xia, T., Zhang, W., Lu, C., Deng, Y., 2017. One-step fabrication of Fe(OH)3@cellulose hollow nanofibers with superior capability for water purification. ACS Appl. Mater. Interfaces 9, 25339-25349. **https://doi.org/ 10.1021/acsami.7b07038**.

Zhou, Y., Zhang, M., Wang, X., Huang, Q., Min, Y., Ma, T., Niu, J., 2014. Removal of crystal violet by a novel cellulose-based adsorbent: comparison with native cellulose. Ind. Eng. Chem. Res. 53, 5498-5506. **https://doi.org/10.1021/ie404135y**.

Zhou, Z., Zhang, X., Lu, C., Lan, L., Yuan, G., 2014. Polyaniline-decorated cellulose aerogel nanocomposite with strong interfacial adhesion and enhanced photocatalytic activity. RSC Adv. 4, 8966-8972. **https://doi.org/10.1039/ c3ra46441e**.